Nanocrystals Hot Paper

How to cite: *Angew. Chem. Int. Ed.* **2022,** *61,* e202201747
International Edition: doi.org/10.1002/anie.202201747
German Edition: doi.org/10.1002/ange.202201747

# Colloidal Bismuth Chalcohalide Nanocrystals

*Danila Quarta[+], Stefano Toso[+], Roberto Giannuzzi, Rocco Caliandro,* Anna Moliterni, Gabriele Saleh, Agostina-Lina Capodilupo, Doriana Debellis, Mirko Prato, Concetta Nobile, Vincenzo Maiorano, Ivan Infante, Giuseppe Gigli, Cinzia Giannini, Liberato Manna, and Carlo Giansante**

**Abstract:** Here we present a colloidal approach to synthesize bismuth chalcohalide nanocrystals (BiEX NCs, in which E = S, Se and X = Cl, Br, I). Our method yields orthorhombic elongated BiEX NCs, with BiSCl crystallizing in a previously unknown polymorph. The BiEX NCs display a composition-dependent band gap spanning the visible spectral range and absorption coefficients exceeding $10^5\ cm^{-1}$. The BiEX NCs show chemical stability at standard laboratory conditions and form colloidal inks in different solvents. These features enable the solution processing of the NCs into robust solid films yielding stable photoelectrochemical current densities under solar-simulated irradiation. Overall, our versatile synthetic protocol may prove valuable in accessing colloidal metal chalcohalide nanomaterials at large and contributes to establish metal chalcohalides as a promising complement to metal chalcogenides and halides for applied nanotechnology.

## Introduction

The pursuit of nontoxic and robust inorganic semiconductors sets bismuth-based materials as promising candidates for light-harvesting purposes[1,2] thanks to a presumably low toxicity[3,4] and a promising (photo)chemical stability.[5,6] Among the most investigated bismuth-based semiconductors stand the oxides, by virtue of their potentially high chemical stability and low cost; however, their wide band gap prevents the absorption of a significant portion of the solar spectrum.[7,8] A more effective sun light absorption can be achieved by the chalcogenides, such as $Bi_2S_3$ and $AgBiS_2$,[9–12] and by the halide double perovskites, such as $Cs_2AgBiBr_6$,[13,14] due to their narrow band gap. Similarly, bismuth chalcohalides have been recognized as potentially efficient solar absorbers,[15–17] with a predicted defect tolerance.[18,19] However, the use of bismuth chalcohalide (nano)materials is still limited and their chemistry remains largely unexplored. Traditional synthetic methods yield good quality single crystals via time- and energy-intensive processes, mostly relying on a slow (up to several days) crystallization upon cooling of a melt from high starting temperatures (up to above 500 °C).[17,20,21] Moreover, the need for a post-growth processing of single crystals limits their use in device fabrication. Indeed, most of the attempts to exploit the light absorption properties of bismuth chalcohalides have been based on their direct growth on conductive substrates, which often resulted in a poor control on the morphology of the synthetic products.[22,23] To overcome these limitations, liquid-phase synthetic approaches have been introduced with the aim of enabling the post-synthesis deposition of the bismuth chalcohalides onto substrates.[24–26] Recently, the issue of processability has been further addressed by colloidal synthetic methods yielding solvent dispersible nanocrystals of $Bi_{13}S_{18}I_2$.[27,28] However, there are no reports to date of the colloidal synthesis of BiSI or related nanomaterials (such as BiSBr or BiSeBr), despite

[*] Dr. D. Quarta,[+] Dr. R. Giannuzzi, Dr. A.-L. Capodilupo, Dr. C. Nobile, Dr. V. Maiorano, Prof. Dr. G. Gigli, Dr. C. Giansante
Consiglio Nazionale delle Ricerche,
Istituto di Nanotecnologia, CNR NANOTEC,
Via Monteroni, 73100 Lecce (Italy)
E-mail: carlo.giansante@nanotec.cnr.it

Dr. D. Quarta,[+] Dr. R. Giannuzzi, Prof. Dr. G. Gigli
Dipartimento di Matematica e Fisica 'Ennio De Giorgi', Università del Salento
Via per Arnesano, 73100 Lecce (Italy)

S. Toso,[+] D. Debellis, Dr. M. Prato, Dr. I. Infante, Dr. L. Manna
Istituto Italiano di Tecnologia, IIT,
Via Morego 30, 16163 Genova (Italy)

S. Toso[+]
International Doctoral Program in Science,
Università Cattolica del Sacro Cuore,
25121 Brescia (Italy)

Dr. R. Caliandro, Dr. A. Moliterni, Dr. C. Giannini
Consiglio Nazionale delle Ricerche,
Istituto di Cristallografia, CNR IC,
Via Amendola 122/O, 70126 Bari (Italy)
E-mail: rocco.caliandro@ic.cnr.it

Dr. G. Saleh
ITMO University, SCAMT Institute,
9 Lomonosova str., 191002 Saint Petersburg (Russian Federation)

[+] Quarta and Toso contributed equally to this work.

them being suggested as potentially efficient, defect tolerant photoactive materials for solar energy conversion purposes.

Here we present a colloidal approach to prepare orthorhombic bismuth chalcohalide nanocrystals (BiEX NCs) via the hot-co-injection of both the chalcogen (E = S, Se) and the halogen (X = Cl, Br, I) precursors to solutions of Bi-carboxylate complexes in a non-coordinating solvent. Following this approach, we have synthesized colloidal BiSCl, BiSBr, BiSI, and BiSeBr NCs; remarkably, BiSCl NCs have been prepared as a previously unknown polymorph. The use of E and X precursors with different reactivities can be exploited to exert control on the size and shape of the BiEX NCs. The as-synthesized BiEX NCs display promising light harvesting properties due to their high absorption coefficients in the Vis spectral range, up to above $10^5$ $cm^{-1}$, and to composition dependent indirect band gaps, ranging between about 1.5 and 2.5 eV. The BiEX NCs show a promising chemical stability at standard laboratory conditions and can withstand temperatures as high as 250 °C in air without decomposing. In addition, the BiEX NCs can form colloidally stable dispersions in solvents of different polarities as a result of post-synthesis surface chemistry modification reactions. These features have enabled the processability of the NC dispersions into robust semiconductor solid films, which can be exploited for, among others, photo(electro)chemical purposes. Indeed, BiSI NC solid films can extract photocurrent densities under prolonged solar-simulated irradiation with a quantum efficiency of the photon-to-current conversion process above 10 % across the entire Vis spectral region.

## Results and Discussion

### Synthesis of the BiEX NCs and Their Morphological, Compositional, and Structural Analysis

Our synthetic approach relied on the reaction of Bi-carboxylate complexes, which were prepared in situ by dissolving bismuth(III) acetate, $Bi(Ac)_3$, in a 1-octadecene solution of oleic acid, with both the S and Br precursors (bis(trimethylsilyl) sulfide, $(Me_3Si)_2S$, and benzoyl bromide, BzBr, respectively), which were introduced in the reaction flask by hot-co-injection. We explicitly avoided the use of complexing agents that may act as reductants (such as oleylamine) to prevent the formation of metallic Bi. Our approach permitted us to tune the Bi:S:Br stoichiometric ratio by independently controlling the corresponding precursor concentration, which is an advantage over the heat-up methods based on the thermal decomposition of metal halide salts.[29] In addition, this approach directly granted access to the chosen reaction temperature, avoiding the formation of undesired phases at lower temperatures.

Upon the co-injection of the S and Br precursors in a 1:2 molar ratio to a Bi-carboxylate solution at 180 °C, a reddish dispersion suddenly formed. A TEM inspection of the reaction product revealed the formation of ribbon-like NCs (Figures 1a, S1 and S2) with a length of about 170 nm and a width of about 20 nm (both with a ≈20 % polydispersity; Figure S3). The XPD and PDF diffraction profiles of the NCs matched the known orthorhombic *Pnam* BiSBr

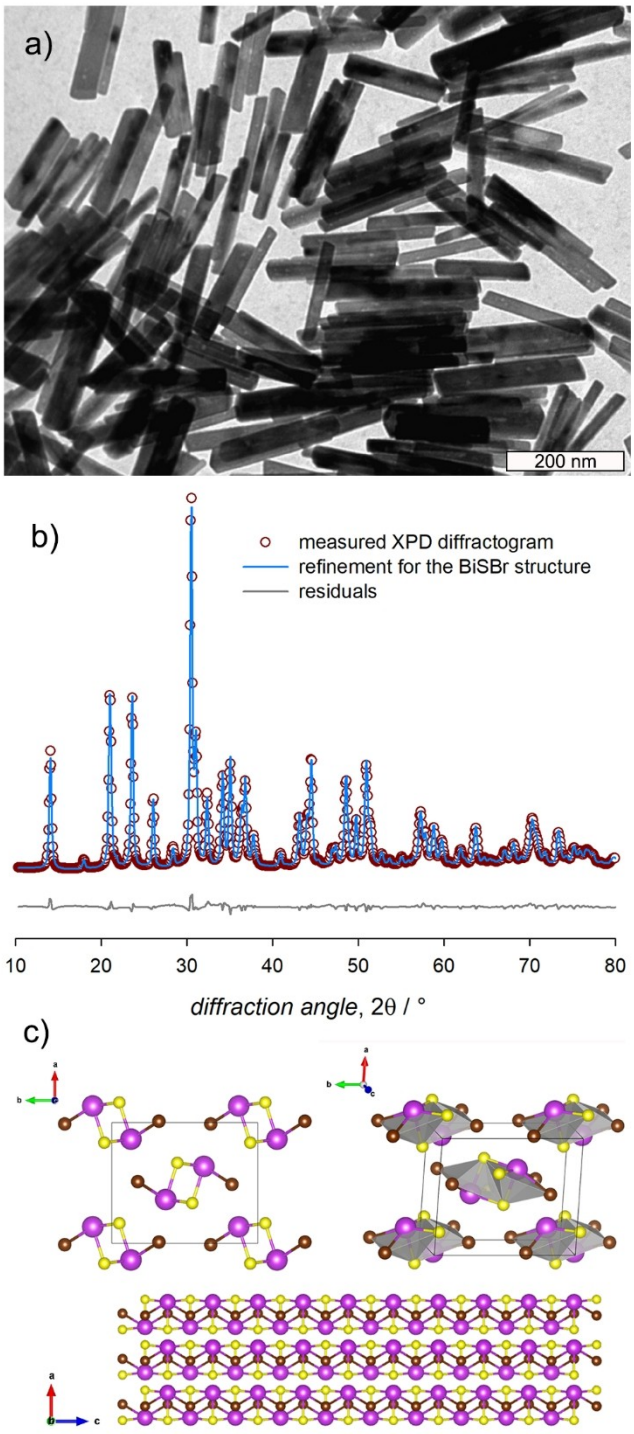


***Figure 1.*** a) TEM image of the as-synthesized BiSBr NCs. b) Rietveld fitting of the synchrotron XPD diffractogram of the BiSBr NCs (to facilitate the comparison with data collected on lab-grade setups, the $2\theta$ values of the XPD horizontal axis were converted to emulate the CuK$\alpha_1$ radiation). c) Crystal structure of the BiSBr NCs highlighting the 1D ribbons along the *c*-axis and the square pyramidal coordination of Bi atoms (according to the CPK coloring: pink is for Bi, yellow is for S, and dark red is for Br).

structure (ICSD-31389,[30] Figures 1b and S4–S6). Upon refinement, the model underwent a 1% variation of the lattice parameters of BiSBr and a negligible average shift of the atomic coordinates. The inclusion of the crystal shape anisotropy factors in the XPD refinement process revealed that the NCs elongate along the *c* axis (Figure S7), indicating that the NC growth may be strongly related to the crystal structure peculiar of BiSBr. Indeed, such a structure features $[(BiSBr)_2]_\infty$ quasi mono-dimensional ribbons constituted by Bi–S frames laterally terminated by Br atoms that are held together by non-covalent interactions. In this arrangement, Bi experiences an edge-sharing square pyramidal coordination, with Bi forming three bonds with S and two bonds with Br (Figure 1c). Compositional analysis revealed that the as-synthesized NCs were Bi-rich and contained almost equivalent amounts of S and Br (XPS data in Figure S8), thus suggesting that the NC surface may be terminated by Bi-oleate complexes.

Starting from this validated synthetic procedure, we tried to achieve synthetic control over the BiSBr NC size and shape. Adjusting the accretion temperature in the 150–210 °C range, following the S and Br precursor co-injection at 180 °C, did not produce significant morphological changes (Figures S9–S12). The attempts to control the NC growth via an eventual ripening induced by changing either the oleic acid concentration or the accretion time mostly resulted in a slight increase of the NC polydispersity (data not shown).

Tuning the reactivity of the synthetic precursors was, instead, a more effective approach to exert control on the NC size and shape; this was accomplished by replacing $(Me_3Si)_2S$ and BzBr with other S and Br precursors, namely 1,1,3,3-tetramethylthiourea and trimethylsilyl bromide, $(Me_3Si)Br$, respectively. The reduced reactivity of tetramethylthiourea (co-injected with either BzBr or $(Me_3Si)Br$) yielded BiSBr NCs with a fairly larger aspect ratio than those obtained with $(Me_3Si)_2S$ (Figures S13–S16). Conversely, we observed that $(Me_3Si)Br$ (when co-injected with $(Me_3Si)_2S$) yielded phase pure BiSBr NCs, showing a lower aspect ratio than that obtained upon co-injecting BzBr and $(Me_3Si)_2S$ (Figures S17 and S18). These findings demonstrated that the use of S and Br precursors with different reactivity can be exploited to control the BiSBr NC morphology, thus further demonstrating the versatility of our synthetic protocol (the aspect ratio distribution of BiSBr NCs obtained with different S and Br precursors is shown in Figure S19).

Our synthetic approach could be extended to the preparation of BiEX NCs other than the BiSBr. As a demonstration, we synthesized colloidal BiSeBr, BiSI, and BiSCl NCs. Upon replacing the S precursor with a Se precursor (1,1-dimethyl-2-selenourea or elemental Se) co-injected with BzBr, we obtained BiSeBr NCs (daylight picture of colloidal dispersions, TEM image, and XRD pattern shown in Figures S20 and S21). Upon replacing the Br precursor with a I precursor (benzoyl iodide, BzI, or trimethylsilyl iodide, $(Me_3Si)I$) co-injected with $(Me_3Si)_2S$, we synthesized darkish colloidal dispersions of BiSI NCs (daylight picture of colloidal dispersions, TEM image, and XRD pattern shown in Figures S22 and S23).

Upon co-injecting benzoyl chloride, BzCl, and $(Me_3Si)_2S$ a yellowish dispersion formed, containing elongated NCs (Figure S24). Remarkably, the XRD pattern of these NCs could not be straightforwardly attributed to any of the known ternary structures in the Bi–S–Cl system (namely, BiSCl[31] and the related disordered structures) nor to any binary combination of these three elements. However, a compositional SEM-EDS analysis of the as-synthesized NCs suggested that we obtained a Bi-rich ternary compound with almost equimolar amounts of S and Cl (Figure S25). The good quality of the XPD data, which featured broad yet well-resolved peaks (Figures 2a and S26), motivated us to attempt an ab-initio structural solution. To this aim, we used the EXPO2014 software:[32] we first determined the unit cell parameters and space group (i.e., the orthorhombic *Pnma*); we then performed the extraction of the integrated inten-

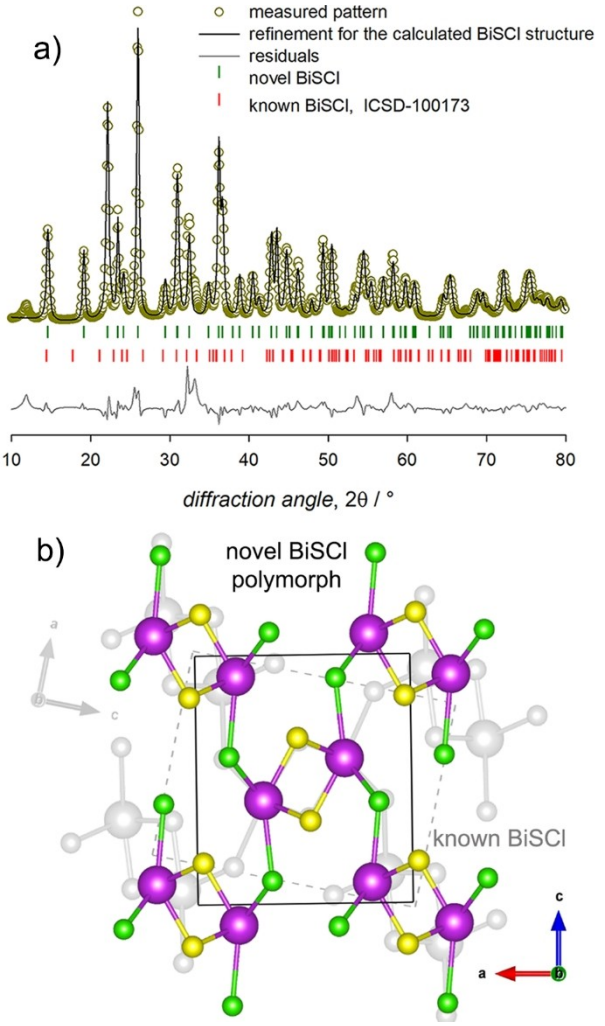


***Figure 2.*** a) Rietveld fit of the XPD data based on the calculated BiSCl model obtained ab-initio and comparison with the reflection list of the known BiSCl structure (to facilitate the comparison with data collected on lab-grade setups, the $2\theta$ values of the XPD horizontal axis were converted to emulate the Cu$K\alpha_1$ radiation). b) Superimposed crystal structures of both the known (grey) and the disclosed (colored) BiSCl polymorphs (according to the CPK coloring: pink is for Bi, yellow is for S, and green is for Cl).

sities for each reflection to achieve the structure solution by direct methods, which provided a structural model that was optimized by a Fourier recycling approach and refined by the Rietveld method (see the Supporting Information for further details). With this approach, we identified a previously unknown polymorph of BiSCl (Figure 2b).[33] This structure shares with the known BiSCl polymorph (and with the other BiSX compounds) the $[(BiSCl)_2]_\infty$ quasi mono-dimensional ribbons held together by non-covalent interactions, which are however arranged differently in the two polymorphs (Figure 2b). Despite the good match of our model with the experimental data, deviations occurred both at large (XPD) and small (PDF) scales due to the presence of minor impurities, as revealed by the presence of non-indexed residual peaks. The contribution of the impurities was estimated as 7% of the total weight by a semi-quantitative analysis of the XPD profile based on the MultiFit approach (see Figure S27).[34] A procedure based on a comparative analysis of the PDF profiles generated from a set of plausible crystal phases did not allow to identify such impurities (Figure S28).

We remark the result of identifying ab initio the crystal structure of our NCs, which is a challenging task, especially on nanomaterials, due to the intrinsic broadening of the diffraction peaks, even if performed on high-quality synchrotron data. As a further confirmation, DFT simulations supported the plausibility of our structural solution, suggesting that this novel BiSCl polymorph is more stable than the previously known polymorph by 10.5 meV atom$^{-1}$ (Table S5). The polymorphism may manifest itself through the color of BiSCl, that is the yellow of our NC dispersions compared to the red of the naturally occurring crystals of BiSCl known as demicheleite-(Cl).[35]

### *Optical Properties and Electronic Structure of the BiEX NCs*

Colloidal BiEX NCs showed composition dependent optical properties, as already evident by a naked eye observation of the yellowish BiSCl, the reddish BiSBr, and the darkish BiSI NC dispersions. The extinction of the incident light (i.e., both absorption and scattering) by toluene dispersions of the BiSX NCs showed a broad peak in the Vis spectral range, which shifted towards lower energies the heavier the X element (Figure 3a). Solid state samples were prepared, by deposition on a glass slide of the as-synthesized NCs, to take into account the scattered light component (characterization of such samples shown in Figures S29–S32). Upon measuring the reflectance and the transmittance of the BiSX NC thin films (Figure S33), along with their thickness, we estimated that the NC absorption coefficients ($\alpha$, Figure S34) exceeded $10^5$ cm$^{-1}$, with larger values the heavier the X element (Figure 3b). Such $\alpha$ values are similar to, if not larger than, those of the methylammonium lead iodide perovskite and other common inorganic semiconductors (Figure S35);[36] in addition, the absorption coefficients of the BiSX NCs are comparable, up to a correction for the dielectric screening exerted by the surrounding ligands and the solvent,[37] to those of the most commonly employed

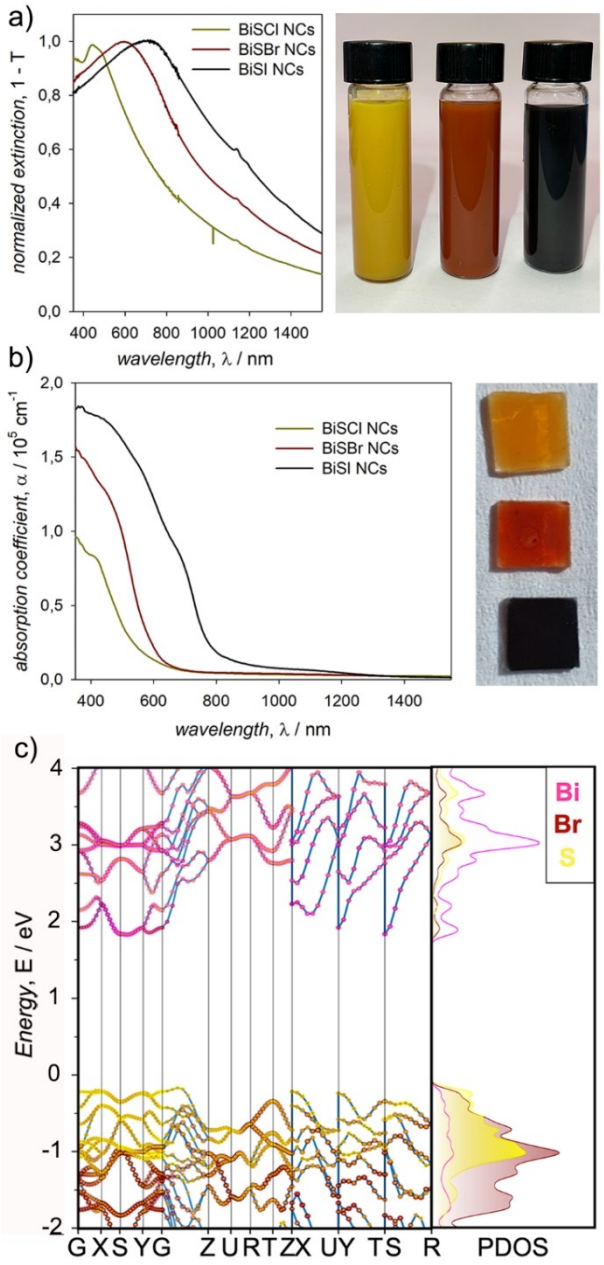


***Figure 3.*** a) Extinction spectra and daylight picture of toluene colloidal dispersions of BiSCl, BiSBr, and BiSI NCs. b) Absorption coefficients and daylight picture of thin films of BiSCl, BiSBr, and BiSI NCs. c) Computed band structure and density of states (with atomic orbital projections) of BiSBr (band structures for BiSCl and BiSI are shown in Figure S39).

colloidal Pb-based NCs, such as chalcogenides and halide perovskites (Figure S36).[38,39] The onset of the absorption spectra was used to estimate the NC indirect band gap, which was 2.05 eV for BiSCl NCs, 1.95 eV for BiSBr NCs, and 1.50 eV for BiSI NCs (Figure S37); the direct band gap of the BiSX NCs, which is expected to be close in energy to the indirect band gap as suggested by the large absorption coefficients, was 2.55 eV for BiSCl NCs, 2.25 eV for BiSBr NCs, and 1.60 eV for BiSI NCs (Figure S38) showing that

the energy difference between the direct and the indirect band gap decreases the heavier the X element (i.e., about 500, 300, and 100 meV for Cl, Br, and I, respectively). No luminescence was detected upon excitation at the low fluences typical of a conventional fluorimeter.

DFT simulations confirmed the indirect character of the band gap and revealed that the valence and conduction band edges are mostly localized on S and Bi atoms, respectively (Figures 3c and S39). The calculated band gaps qualitatively reproduced the experimental trend of the BiSX NCs, namely: 2.15 eV, 2.00 eV, and 1.82 eV for X = Cl, Br, and I, respectively. However, a quantitative comparison with the experimental values is affected both by the well-known tendency of GGA functionals (such as PBE) to underestimate the band gap and by the overestimation due to the neglect of SOC effects. In fact, the inclusion of SOC led to a band gap reduction (from 2.00 to 1.50 eV for BiSBr), without modifying the indirect character of the lowest energy electronic transition (Figure S40). Nevertheless, DFT calculations were useful to estimate the impact of polymorphism on the optical properties of BiSCl: accordingly, the estimated band gap of the known BiSCl polymorph was 1.83 eV, i.e. about 300 meV smaller than that of our BiSCl NCs (Figure S41); these calculated band gap values may explain the appreciable color differences between our yellow NCs and the red demicheleite-(Cl) crystals (Figure S42).[35]

### *Stability of the BiEX NCs*

The reliability of our synthetic method prompted us to test the stability and processability of our BiEX NCs, which are fundamental for potential applications. To this aim, we prevalently investigated the BiSBr NCs, although we extended such an investigation to the other BiEX NCs. Toluene dispersions and dry powders of the NCs showed no appreciable differences in their XRD patterns upon long term storage at ambient conditions. The BiSBr NCs underwent a slight oxidation only when the thin film samples prepared for XRD measurements were aged in ambient conditions for one month at least (Figures 4a and S43). In addition, no further structural transformation could be observed upon annealing the NCs in air up to 250 °C; above this temperature, the BiSBr NCs started to convert to the oxybromide BiOBr (Figure 4a). In the perspective of device fabrication, such a thermal stability could be exploited to anneal the NCs casted onto a substrate to eventually induce close packing, which may promote inter-NC electronic coupling.

The as-synthesized NCs showed a Bi-rich composition, thus suggesting that their surface may be terminated by Bi-oleate complexes. The oleyl chains exposed to the surroundings conferred a decent colloidal stability to the NCs. However, the NC length, often exceeding 100 nm, and the tendency to bundle of elongated NCs, caused their precipitation and the eventual adhesion to the glass walls of the dispersion containers. In order to solve this issue, we performed post-synthesis surface chemistry modification

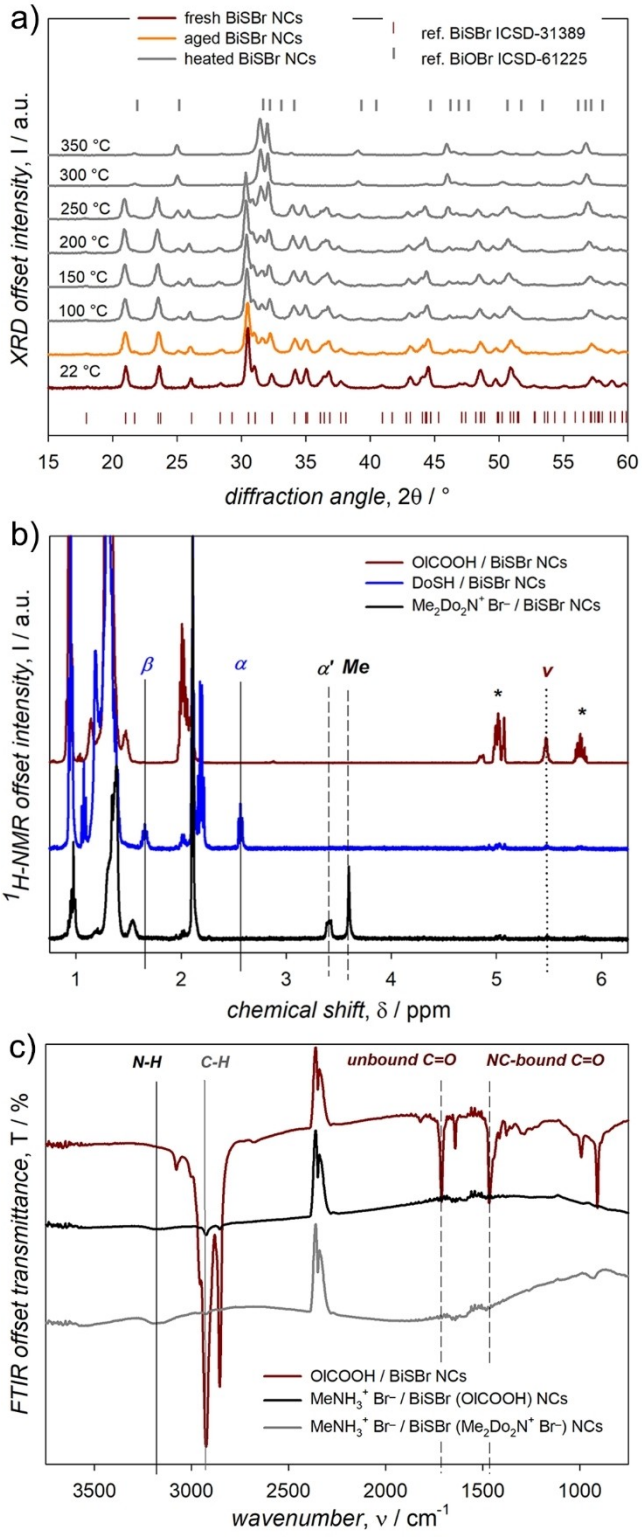


***Figure 4.*** a) XRD patterns of the BiSBr NCs upon one month storage at ambient conditions then heated up to 350 °C. b) 1H NMR spectra of the as-synthesized BiSBr NCs upon ligand exchange with either 1-dodecanethiol or dimethyldidodecylammonium bromide in toluene-d8. c) FTIR spectra of the BiSBr NCs capped with either oleic acid or dimethyldidodecylammonium bromide upon solution phase ligand exchange with methylammonium bromide.

reactions by the room temperature addition of ligands that were expected to bind surface Bi atoms.[40] We thus used ligands with an aliphatic pendant moiety and a binding moiety constituted by the same non-metal elements of the NCs, namely the S of 1-dodecanethiol (DoSH) and the Br of dimethyldidodecylammonium bromide ($Me_2Do_2N^+Br^-$). As shown by $^1H$ NMR measurements, both ligands quantitatively displaced the oleate ligands coming from the synthetic procedures (Figure 4b). Indeed, the replacing ligand addition and the subsequent NC purification resulted in an almost complete disappearance of the vinylene resonance of the oleyl moiety at ≈5.4 ppm and in the concomitant appearance of resonances characteristic of either aliphatic thiols or quaternary ammonium salts (Figure 4b).

The replacing ligands improved the colloidal stability of both the BiSBr NC dispersions, although an excess of such ligands, as suggested by the narrow linewidth and the multiplicity of the NMR resonances,[41] was necessary to achieve long-term stability (Figure S44). In particular, NCs coordinated by $Me_2Do_2N^+Br^-$ ligands could be readily redispersed in apolar solvents, such as toluene, by gentle shaking with no appreciable amount of material sticking to the glass vial walls. In addition, the replacing ligands did not induce structural transformations in both the BiSBr NCs, which is instead a common observation for metal halide perovskite NCs (Figure S45).[39] We also used ammonium halide salts with short aliphatic substituents (such as methylammonium bromide, $MeNH_3^+Br^-$) with the intent of promoting inter-NC electronic coupling in solids thereof. Indeed, $MeNH_3^+Br^-$ ligands could effectively coordinate the NC surface, permitting to transfer the BiSBr NCs in polar solvents, such as dimethylformamide. The $MeNH_3^+Br^-$ species efficiently replaced either the pristine oleate ligands from the NC surface, as shown by FTIR measurements: the carbonyl stretching of NC-bound oleate at ≈1470 $cm^{-1}$ (and that of the excess oleic acid appearing at ≈1700 $cm^{-1}$) almost disappeared upon $MeNH_3^+Br^-$ exchange and transfer to dimethylformamide, accompanied by a drastic reduction of C–H stretching at ≈2900 $cm^{-1}$; in addition, a broad peak appeared at ≈3200 $cm^{-1}$ that was assigned to N–H stretching (Figure 4c). An efficient ligand exchange to $MeNH_3^+Br^-$ was achieved also starting from NCs capped with $Me_2Do_2N^+Br^-$ (Figure 4c); this is of particular importance for the fabrication of NC solids with an appreciable inter-NC charge transport (as described hereinafter).

### *Towards Photoelectrochemical Applications of the BiEX NCs*

The promising light absorption properties of the BiEX NCs and the amenability to both surface chemistry modification and thermal annealing permitted us to process the NCs into stable, insoluble solids that can be deposited on various substrates (such as bare glasses, conductive glasses, stainless steel, and silicon wafers). Such solids were fabricated by a three-step method comprising: *i*) the spin casting of the NCs previously exchanged in the solution phase with the corresponding $Me_2Do_2N^+X^-$ salt; *ii*) the solid phase exchange of the ligands with the corresponding $MeNH_3^+X^-$ salt, then followed by rinsing with dimethylformamide; *iii*) the thermal annealing at 180 °C. All the steps were repeated up to eight times to fill cracks and voids due to the displacement of the bulky ligands and to the eventual close packing of the NCs induced by the annealing process. We point out that such a procedure to fabricate NC solid films was conducted at standard laboratory conditions, without control on either the ambient temperature or humidity. In the case of BiSI, we obtained NC solid films with a metallic luster (Figure 5a) and a reduced rugosity, as demonstrated by the variations in thickness amplitude (±7 %) measured both at the mesoscopic size scale, with a profilometer, and at the microscopic size scale, by SEM imaging (Figures S46 and S47). Morphological, compositional, and structural analysis of the solid films revealed that the BiSI NCs were negligibly affected by the photoelectrode fabrication procedure com-

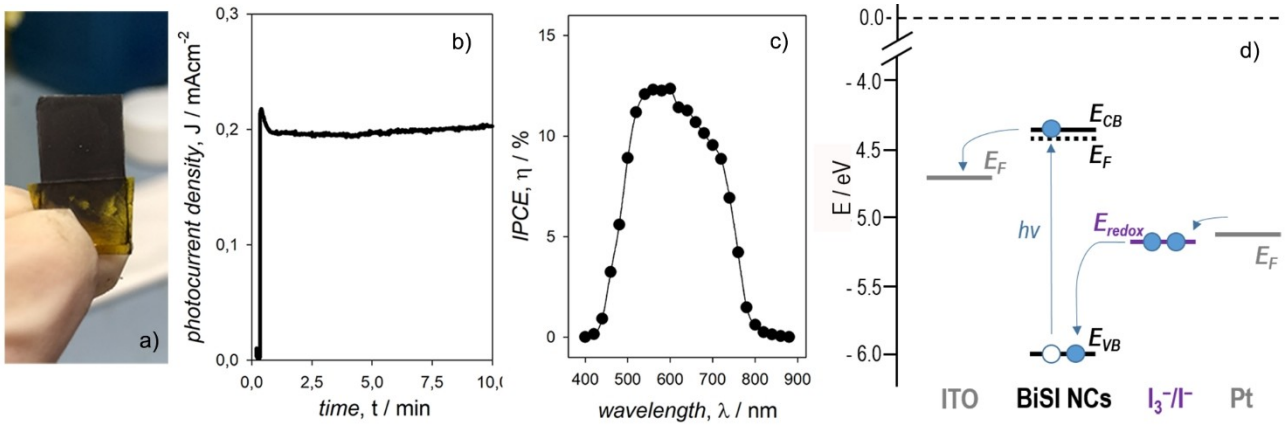


***Figure 5.*** a) Daylight picture of a BiSI NC film cast on a ITO substrate used as a working electrode for photoelectrochemical measurements. b) Photocurrent density extracted at a 0.25 V bias under solar-simulated illumination. c) Incident photon to current conversion efficiency at a 0.25 V bias under monochromatic illumination. d) Tentative energy level diagram of the photoelectrochemical cell based on BiSI NC photoelectrodes.

prising a double ligand exchange and an annealing step (SEM-EDS, XPS, and XRD data are shown as Figures S48–S50, respectively).

We thus performed photoelectrochemical studies by using BiSI NC solids deposited on conductive (ITO) substrates as the working electrode (Figure 5a), which was immersed in an electrolytic solution containing the iodine/iodide redox couple; the current passing through the NC solids was balanced at a Pt plate as counter electrode, while the potential was controlled with an Ag/AgCl reference electrode (Figure S51).[42] Under solar simulated illumination, a photocurrent density of the order of the $mA\,cm^{-2}$ was extracted at a 0.25 V bias; after a slight initial drop, most likely related to the photo-induced occupation of trap states, a stable photocurrent density could be extracted for several minutes, with a good reproducibility between different NC solids (Figures 5b and S52). Chopped-light current density-voltage measurements were used to estimate the flat band potential of the BiSI NC solids,[43] which we estimated at −4.6 eV vs the vacuum level (Figure S53). The quantum efficiency of the incident photon energy conversion to extracted charge carriers (IPCE, η) was evaluated, in the same three-electrode configuration, to be above 10 % across the entire Vis spectral range (Figures 5c, S54, and S55). Electrochemical impedance measurements were carried out to identify the n-type semiconducting behavior of the BiSI NC solids via the Mott–Schottky analysis (Figure S56).[44] The n-type character of the BiSI NC films was corroborated by UPS measurements, which suggested that the Fermi level lies close to the conduction band edge, being the absolute energy of the valence band edge at −6.00 eV vs the vacuum level and the work function of ≈4.35 eV (Figure S57). Considered also the work functions of both the ITO substrate[45] and the Pt plate[46] together with the redox potential of the $I_3^-/I^-$ couple,[47] an energy level diagram was attempted (Figure 5d). We note that our BiSI NC solids were stable all throughout the measurements and did not show appreciable signs of degradation upon intense ($100\,mW\,cm^{-2}$) irradiation in the corrosive environment of an electrolytic solution containing the iodine/iodide redox couple. Such a robustness of our NC solids is remarkable, considering that photoelectrochemical measurements in analogous experimental conditions on Pb chalcogenide and halide perovskite NCs are often unfeasible due to their degradation.

## Conclusion

Here we have presented a synthetic method to prepare colloidal orthorhombic BiEX NCs. Our method is based on the hot-co-injection of both the chalcogen and halogen precursors in a Bi-carboxylate complex solution. The crystal structure peculiar of BiEX, which features a directional Bi–S covalent framework, prompts the growth of elongated NCs. Different chalcogen and halogen precursors proved able to exert control on the aspect ratio of the NCs. Our method may be further consolidated by the use of precursor libraries[48] to systematically pursue the tuning of the NC size and shape; we also expect that our synthetic protocol could be reliably applied to other pnictogen cations, such as As and Sb, and to mixed metal, quaternary chalcohalide, such as those comprising other cations like Ag, Cu, Cs, among others. To the best of our knowledge, this is the first report on the synthesis of colloidal orthorhombic BiEX NCs. Interestingly, the BiSCl NCs crystallized only in a previously unknown polymorph, thus confirming how the colloidal synthesis of nanoscopic crystals may give access to phases that cannot be stabilized at larger size scales.[29,49,50] The colloidal Bi chalcohalide NCs showed composition dependent band gaps and large optical absorption coefficients across the Vis spectral range, comparable to those of other semiconductors such as the Pb chalcogenides and halide perovskites. The colloidal BiEX NCs can be processed from the solution phase at ambient conditions without significant degradation: both surface chemistry modification and thermal annealing were exploited to prepare robust NC solids that can withstand photocorrosion more than the Pb chalcogenides and halide perovskite NCs. We thus fabricated photoelectrodes based on our BiEX NCs that can harvest the sun light extracting an electric current with a quantum efficiency above 10 % across the entire Vis spectral range. We expect further improvements for vertical devices that could potentially take advantage of the directional Bi–S framework of the NCs.[51,52] These findings set the colloidal BiEX NCs as promising solar absorbers for photocatalytic and optoelectronic applications.[23,53,54] This work thus extends our knowledge on the chemistry of metal chalcohalide nanomaterials and contributes to establish this class of inorganic semiconductors as an effective complement to metal chalcogenides and halides for light-harvesting purposes.

## Acknowledgements

The authors thank Dr. A. Balena for assistance with the profilometer and Dr. C. Chiarella and G. Filograsso for administrative support. We acknowledge the CINECA award under the ISCRA initiative, for the availability of high-performance computing resources and support. Open Access Funding provided by Consiglio Nazionale delle Ricerche within the CRUI-CARE Agreement.

## Conflict of Interest

C.Gians., D.Q., S.T., R.G., R.C., A.M., C.Giann., L.M., G.G. are co-inventors on a patent application entitled “Process for the Production of Nanocrystals of Metal Chalcohalides”, IT 102022000001577.

## Data Availability Statement

The data that support the findings of this study are available from the corresponding author upon reasonable request.

**Keywords:** Bismuth Chalcohalides · Colloidal Synthesis · Light-Harvesting · Nanocrystals · Photoelectrochemistry


[1] X. Meng, Z. Zhang, *J. Mol. Catal. A* **2016**, *423*, 533.
[2] F. Palazon, *Solar RRL* **2022**, *6*, 2100829.
[3] H. Suzuki, N. Komatsu, T. Ogawa, T. Murafuji, T. Ikegami, Y. Matano, *Organobismuth Chemistry*, Elsevier, Amsterdam, **2001**.
[4] R. Mohan, *Nat. Chem.* **2010**, *2*, 336.
[5] F. M. Toma, J. K. Cooper, V. Kunzelmann, M. T. McDowell, J. Yu, D. M. Larson, N. J. Borys, C. Abelyan, J. W. Beeman, K. Man Yu, J. Yang, L. Chen, M. R. Shaner, J. Spurgeon, F. A. Houle, K. A. Persson, I. D. Sharp, *Nat. Commun.* **2016**, *7*, 12012.
[6] N. C. Miller, M. Bernachea, *APL Mater.* **2018**, *6*, 084503.
[7] Y. Qiu, M. Yang, H. Fan, Y. Zuo, Y. Shao, Y. Xu, X. Yanga, S. Yang, *CrystEngComm* **2011**, *13*, 1843.
[8] A. Walsh, G. W. Watson, D. J. Payne, R. G. Edgell, J. Guo, P.-A. Glans, T. Learmonth, K. E. Smith, *Phys. Rev. B* **2006**, *73*, 235104.
[9] A. D. Schricker, M. B. Sigman, B. A. Korgel, *Nanotechnology* **2005**, *16*, S508.
[10] L. Cademartiri, R. Malakooti, P. G. O'Brien, A. Migliori, S. Petrov, N. P. Kherani, G. A. Ozin, *Angew. Chem. Int. Ed.* **2008**, *47*, 3814; *Angew. Chem.* **2008**, *120*, 3874.
[11] S. N. Guin, K. Biswas, *Chem. Mater.* **2013**, *25*, 3225.
[12] M. Bernechea, N. C. Miller, G. Xercavins, D. So, A. Stavrinadis, G. Konstantatos, *Nat. Photonics* **2016**, *10*, 521.
[13] E. Greul, M. L. Petrus, A. Binek, P. Docampo, T. Bein, *J. Mater. Chem. A* **2017**, *5*, 19972.
[14] Y. Zhang, T. Shah, F. L. Deepak, B. A. Korgel, *Chem. Mater.* **2019**, *31*, 7962.
[15] N. T. Hahn, J. L. Self, C. B. Mullins, *J. Phys. Chem. Lett.* **2012**, *3*, 1571.
[16] D. Tiwari, F. Cardoso-Delgado, D. Alibhai, M. Mombrú, D. J. Fermín, *ACS Appl. Energy Mater.* **2019**, *2*, 3878.
[17] E. Wlaźlak, A. Blachecki, M. Bisztyga-Szklarz, S. Klejna, T. Mazur, K. Mech, K. Pilarczyk, D. Przyczyna, M. Suchecki, P. Zawalad, K. Szaciłowski, *Chem. Commun.* **2018**, *54*, 12133.
[18] R. E. Brandt, V. Stevanović, D. S. Ginley, T. Buonassisi, *MRS Commun.* **2015**, *5*, 265.
[19] A. M. Ganose, S. Matsumoto, J. Buckeridge, D. O. Scanlon, *Chem. Mater.* **2018**, *30*, 3827.
[20] M. V. Moroz, M. V. Prokhorenko, *Inorg. Mater.* **2016**, *52*, 765.
[21] R. Ganesha, D. Arivuoli, P. Ramasamy, *J. Cryst. Growth* **1993**, *128*, 1081.
[22] S. Li, L. Xu, X. Kong, T. Kusunose, N. Tsurumachia, Q. Feng, *J. Mater. Chem. C* **2020**, *8*, 3821.
[23] S. Farooq, T. Feeney, J. O. Mendes, V. Krishnamurthi, S. Walia, E. Della Gaspera, J. van Embden, *Adv. Funct. Mater.* **2021**, *31*, 2104788.
[24] L. Zhu, Y. Xie, X. Zheng, X. Yin, X. Tian, *Inorg. Chem.* **2002**, *41*, 4560.
[25] H. Kunioku, M. Higashi, R. Abe, *Sci. Rep.* **2016**, *6*, 32664.
[26] H. Sun, G. Yang, J. Chen, C. Kirk, N. Robertson, *J. Mater. Chem. C* **2020**, *8*, 13253.
[27] B. Xu, T. Feng, M. T. Agne, Q. Tan, Z. Li, K. Imasato, L. Zhou, J.-H. Bahk, X. Ruan, G. J. Snyder, Y. Wu, *Angew. Chem. Int. Ed.* **2018**, *57*, 2413; *Angew. Chem.* **2018**, *130*, 2437.
[28] Y. Wu, H. Pan, X. Zhou, M. Li, B. Zhou, C. Yang, W.-H. Zhang, J. Jie, C. Li, *Chem. Sci.* **2015**, *6*, 4615.
[29] S. Toso, Q. A. Akkerman, B. Martín-García, M. Prato, J. Zito, I. Infante, Z. Dang, A. Moliterni, C. Giannini, E. Bladt, I. Lobato, J. Ramade, S. Bals, J. Buha, D. Spirito, E. Mugnaioli, M. Gemmi, L. Manna, *J. Am. Chem. Soc.* **2020**, *142*, 10198.
[30] G. P. Voutsas, P. J. Rentzeperis, *Z. Kristallogr.* **1984**, *166*, 153.
[31] G. P. Voutsas, P. J. Rentzeperis, *Z. Kristallogr.* **1980**, *152*, 109.
[32] A. Altomare, C. Cuocci, C. Giacovazzo, A. Moliterni, R. Rizzi, N. Corriero, A. Falcicchio, *J. Appl. Cryst.* **2013**, *46*, 1231.
[33] Cystallographic data of the new polymorph of BiSCl are deposited at the Cambridge Crystallographic Data Centre (CCDC) with deposition number 2154418. These data are provided free of charge by the joint Cambridge Crystallographic Data Centre and Fachinformationszentrum Karlsruhe Access Structures service.
[34] R. Caliandro, B. D. Belviso, *J. Appl. Cryst.* **2014**, *47*, 1087.
[35] F. Demartin, C. M. Gramaccioli, I. Campostrini, *Am. Mineral.* **2009**, *94*, 1045.
[36] S. De Wolf, J. Holovsky, S.-J. Moon, P. Löper, B. Niesen, M. Ledinsky, F. J. Haug, J. H. Yum, C. Ballif, *J. Phys. Chem. Lett.* **2014**, *5*, 1035.
[37] Z. Hens, I. Moreels, *J. Mater. Chem.* **2012**, *22*, 10406.
[38] D. Debellis, G. Gigli, S. ten Brinck, I. Infante, C. Giansante, *Nano Lett.* **2017**, *17*, 1248.
[39] D. Quarta, M. Imran, A.-L. Capodilupo, U. Petralanda, B. van Beek, F. De Angelis, L. Manna, I. Infante, L. De Trizio, C. Giansante, *J. Phys. Chem. Lett.* **2019**, *10*, 3715.
[40] C. Giansante, *Acc. Chem. Res.* **2020**, *53*, 1458.
[41] R. Grisorio, D. Debellis, G. P. Suranna, G. Gigli, C. Giansante, *Angew. Chem. Int. Ed.* **2016**, *55*, 6628; *Angew. Chem.* **2016**, *128*, 6740.
[42] G. Boschloo, D. Fitzmaurice, *J. Phys. Chem. B* **1999**, *103*, 2228.
[43] A. Hankin, F. E. Bedoya-Lora, J. C. Alexander, A. Regoutz, G. H. Kelsall, *J. Mater. Chem. A* **2019**, *7*, 26162.
[44] F. Cardon, W. P. Gomes, *J. Phys. D* **1978**, *11*, L63.
[45] R. Schlaf, H. Murata, Z. H. Kafaf, *J. Electron Spectrosc. Relat. Phenom.* **2001**, *120*, 149.
[46] H. B. Michaelson, *J. Appl. Phys.* **1977**, *48*, 4729.
[47] G. Boschloo, A. Hagfeldt, *Acc. Chem. Res.* **2009**, *42*, 1819.
[48] M. P. Hendricks, M. P. Campos, G. T. Cleveland, I. Jen-La Plante, J. S. Owen, *Science* **2015**, *348*, 1226.
[49] B. A. Tappan, R. L. Brutchey, *ChemNanoMat* **2020**, *6*, 1567.
[50] F. Therrien, E. B. Jones, V. Stevanovic, *Appl. Phys. Rev.* **2021**, *8*, 031310.
[51] W. U. Huynh, J. J. Dittmer, A. P. Alivisatos, *Science* **2002**, *295*, 2425.
[52] H. Shi, W. Ming, M.-H. Du, *Phys. Rev. B* **2016**, *93*, 104108.
[53] J. Li, W. Pan, Q. Liu, Z. Chen, Z. Chen, X. Feng, H. Chen, *J. Am. Chem. Soc.* **2021**, *143*, 6551.
[54] S. Li, L. Xu, X. Kong, T. Kusunose, N. Tsurumach, Q. Feng, *ChemSusChem* **2021**, *14*, 3351.


Manuscript received: January 31, 2022
Accepted manuscript online: February 28, 2022
Version of record online: March 10, 2022